

# Synthesis of titanium dioxide–reduced graphite oxide nanocomposites and their photocatalytic performance

Ying He, Yihe Zhang, Hongwei Huang, Rui Zhang

National Laboratory of Mineral Materials, School of Materials Science and Technology, China University of Geosciences, Beijing 100083, People's Republic of China  
E-mail: zyh@cugb.edu.cn

Published in Micro & Nano Letters; Received on 31st March 2013; Revised on 22nd July 2013; Accepted on 26th July 2013

Chemically bonded titanium dioxide (TiO<sub>2</sub>)–reduced graphite oxide (RGO) composites have been successfully prepared with graphite oxide and peroxotitanium complex by low-temperature liquid reaction. The prepared TiO<sub>2</sub> nanoparticles with diameters of about 10 nm consisted of anatase phase and a slight amount of brookite phase. In the TiO<sub>2</sub>–RGO composites, TiO<sub>2</sub> nanoparticles were uniformly dispersed on the RGO surface from the scanning electron microscopy images. The as-prepared TiO<sub>2</sub>–RGO composites exhibited much higher efficiency in the degradation of methylene blue under ultraviolet light irradiation compared with pure TiO<sub>2</sub> nanoparticles. In addition, the influences of the RGO content in the TiO<sub>2</sub>–RGO composites on the photocatalytic degradation activity were also researched.

**1. Introduction:** Semiconductor photocatalytic materials have been intensively investigated for photocatalytic degradation of organic pollutants during the past decades [1]. Among various oxide photocatalysts, titanium dioxide (TiO<sub>2</sub>) has been proved to be the most promising material for its superior photocatalytic performance, low cost, non-toxicity and long-term stability against photo and chemical corrosion [2–4]. However, in TiO<sub>2</sub> nanoparticles several problems exist when using them as photocatalysts, such as easy aggregation, difficulty to separate from the aqueous solution and easy recombination of photoinduced electrons and holes. Thus, the immobilisation of TiO<sub>2</sub> has been a crucial problem in photocatalytic technology. In recent years, the composites of TiO<sub>2</sub> and carbon materials (TiO<sub>2</sub>–C) have been considered as potential photocatalysts for water purification [5]. In TiO<sub>2</sub>–C composites, carbon materials acting as supporting materials can be generally categorised into four kinds: TiO<sub>2</sub>–activated carbon, TiO<sub>2</sub>–fullerene (C<sub>60</sub>), TiO<sub>2</sub>–graphene and TiO<sub>2</sub>–carbon nanotubes [6–8]. Each exhibits good photocatalytic activity. It is of great significance to obtain a TiO<sub>2</sub>–C composite possessing photocatalytic activity beyond TiO<sub>2</sub>.

Graphite oxide (GO) is a two-dimensional layered compound. Owing to the introduction of oxygen-containing functional groups (hydroxyl, carboxyl and epoxy groups) on carbon nanosheets, GO disperses well in water under ultrasonic treatment and forms a stable colloidal solution. Moreover, the GO is active and easily absorbs polar molecules to form different composites [9, 10].

In this Letter, we present a simple method to prepare TiO<sub>2</sub>–reduced GO (RGO) composites as photocatalysts with GO and peroxotitanium complex (PTC) under a low temperature liquid reaction. The PTC served as a reducing agent for GO and no extra reducing agent was required, which made the process simple. Without high temperature processing, the as-prepared TiO<sub>2</sub> nanoparticles in the composites adopted anatase phase and were uniformly loaded on the surface of reduced GO with a chemical bond. The TiO<sub>2</sub>–RGO composites prepared by this method exhibited high photocatalytic activity. The effects of different amounts of RGO on photocatalytic degradation activity in the composites are discussed. The structures of the resultant composites were characterised by X-ray diffraction (XRD), scanning electron microscopy (SEM), transmission electron microscopy (TEM) and Fourier transform infrared (FTIR). The photocatalytic activities of the as-prepared samples were tested on degrading methylene blue (MB) dyes under UV light irradiation.

## 2. Experiments

**2.1. Synthesis of GO:** GO was obtained according to the modified method reported by Hammers and Offeman [11]. In brief, 2.5 g of flake graphite powder and 1.25 g of NaNO<sub>3</sub> dispersed in 60 ml of H<sub>2</sub>SO<sub>4</sub> were kept at 0°C with vigorous stirring. Then, 7.5 g of KMnO<sub>4</sub> was slowly added. After the solution formed a well-mixed slurry, it was transferred to a 35°C water bath and stirred for 1.5 h. The temperature was raised to 98°C after the addition of 125 ml of distilled water. The solution changed to a brown colour during the dropwise addition of 5 ml of 30% H<sub>2</sub>O<sub>2</sub>. The solution was filtered and then washed with 5% HCl and distilled water several times. Finally, the filter cake was dried in vacuum at 40°C.

**2.2. Preparation of TiO<sub>2</sub>–RGO composites:** TiCl<sub>4</sub> (3 ml) was slowly added into distilled water (270 ml) under constant stirring for 30 min until it was completely dissolved. An aqueous solution of NH<sub>4</sub>OH (2.5 wt%) was then added to form white titanium hydroxide gel under vigorous stirring until the pH was 7. After ageing for 12 h, titanium hydroxide gel was filtered and washed with distilled water until no Cl<sup>–</sup> were detected with AgNO<sub>3</sub> in the solution. Distilled water was then added to the titanium hydroxide white gel cake. GO was dissolved in distilled water by ultrasonic treatment for 15 min and then added to titanium hydroxide gel with stirring to obtain a homogeneous suspension. The aqueous solution of H<sub>2</sub>O<sub>2</sub> (30 wt%) was then added gradually with vigorous stirring to form a mixed suspension of GO and PTC. The resulting suspension was heated at 98°C for 12 h and then dried at 70°C. The content of GO in the composite was tuned by changing the concentration of the added GO suspension. Pure TiO<sub>2</sub> was prepared with the same procedure but without the addition of GO.

**2.3. Photocatalytic experiment:** A 50 mg TiO<sub>2</sub>–RGO composite was dispersed in an aqueous solution of the MB dyes (150 ml 20 mg/l), the suspensions were magnetically stirred in the dark for 45 min to obtain adsorption–desorption equilibration, and then the TiO<sub>2</sub>–RGO particles were collected by filtration for the next photocatalytic experiment. In the test, 150 ml of MB solution (5 mg/l) and 50 mg TiO<sub>2</sub>–RGO photocatalyst were placed in a reactor (250 ml) with stirring. A UV lamp ( $\lambda = 254$  nm) was positioned about 20 cm above the photoreactor. After stirring for 15 min in the dark, the photocatalytic reaction was started by

turning on the UV lamp. At given time intervals, 5 ml of the liquid was sampled and analysed by recording absorbance at the characteristic band of 665 nm using a Cary 5000 UV-visible spectrophotometer.

**2.4. Characterisation and analysis:** Powder XRD was performed on an X/max-rA Advance with Cu K $\alpha$  radiation. FTIR spectra were carried out using a Perkin-Elmer spectrometer in the frequency range of 4000–500 cm<sup>-1</sup>. The SEM images were taken using an S-4800 electron microscope. The morphology of the particles was observed by TEM using a JEOL 2010 instrument at 200 kV.

**3. Results and discussion:** Fig. 1 shows the XRD pattern of GO, TiO<sub>2</sub>-RGO and TiO<sub>2</sub>, respectively. From the XRD pattern of GO, it could be seen that there was a strong and sharp diffraction peak at 2 $\theta$  of 11.6°, which was attributed to the (001) characteristic diffraction peak of the GO. In Fig. 1, TiO<sub>2</sub>-RGO and TiO<sub>2</sub> shows a similar XRD pattern with pure anatase-TiO<sub>2</sub> and the diffraction peak at 2 $\theta$  of 30.7° is indexed to the brookite phase (121). However, no diffraction peaks of carbon species can be observed in TiO<sub>2</sub>-RGO, possibly because of the relatively low content of RGO in the composites, which was covered by the diffraction signals of TiO<sub>2</sub> [12].

The FTIR spectra of the as-prepared GO, TiO<sub>2</sub>-RGO and TiO<sub>2</sub> is displayed in Fig. 2. GO (curve 1) shows the characteristic absorption peak at 1732 cm<sup>-1</sup> (C=O stretching vibration from COOH groups), 1410 cm<sup>-1</sup> (C–OH stretching vibrations of COOH groups), 1228 cm<sup>-1</sup> (epoxy stretching vibration) and 1030 cm<sup>-1</sup> (alkoxy stretching vibration), which provides the evidence for the presence of different types of oxygen-containing functional groups including –COOH, –C–OH, –C=O and epoxy groups on the GO. The as-prepared TiO<sub>2</sub> (curve 3) shows a low frequency

band of about 670 cm<sup>-1</sup>, which corresponds to the vibration of Ti–O–Ti bonds. The peaks at 1630 and 1400 cm<sup>-1</sup> are attributed to O–H bending vibration from absorbed H<sub>2</sub>O and the stretching vibration of the N–H bonds in NH<sub>4</sub><sup>+</sup> remained, respectively in [13]. The broad absorption of about 3500–3100 cm<sup>-1</sup> was assigned to O–H stretching vibration from surface –OH groups of TiO<sub>2</sub>. For the TiO<sub>2</sub>-RGO (curve 2), the new peaks at 1610 cm<sup>-1</sup> are attributed to the aromatic –C=C– bonds of the RGO network. Moreover, in the spectrum of TiO<sub>2</sub>-RGO, the peak assigned to the oxygen functional groups disappears, indicating the reduction of GO by the hydrothermal treatment and redox reaction between the titanium precursor and the GO. However, in the as-prepared TiO<sub>2</sub>-RGO, the broad absorption below 1000 cm<sup>-1</sup> is larger than the corresponding peak in TiO<sub>2</sub> and shifts towards a high wavenumber. In fact, this peak could be looked as a combination of Ti–O–Ti vibration and Ti–O–C vibration (798 cm<sup>-1</sup>) [14]. The presence of Ti–O–C bonds suggests that the –COOH moieties groups on the GO surface firmly interacted with the surface –OH groups of TiO<sub>2</sub> particles. Furthermore, the carboxyl group of GO could also coordinate with the titania surface through the bridging bidentate mode [15]. Thus, TiO<sub>2</sub> particles were chemically bonded onto the RGO surface.

Fig. 3 demonstrates the SEM images of the GO and the TiO<sub>2</sub>-RGO with different GO concentrations. The as-prepared GO was composed of several sheets and maintained a layered structure with micrometres-long wrinkles on the surface. The SEM images of the TiO<sub>2</sub>-RGO composites (Fig. 3b) revealed dense TiO<sub>2</sub> nanoparticles bound to the RGO surface and most TiO<sub>2</sub> nanoparticles were distributed with aggregation. However, there are no obvious particles loading on the TGO surface (Fig. 3c). Fig. 3c shows that

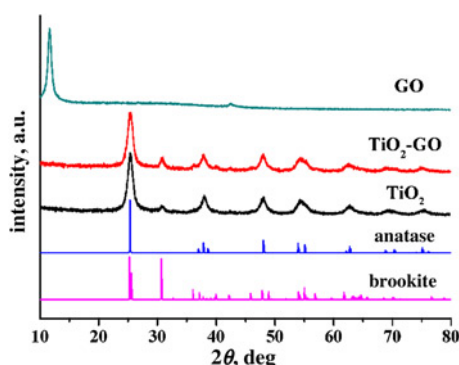


**Figure 1** XRD patterns of as-prepared GO, TiO<sub>2</sub>-RGO, TiO<sub>2</sub> and the anatase TiO<sub>2</sub> (JCPDS 78-2468) and brookite TiO<sub>2</sub> (JCPDS 76-1937) are also shown as references

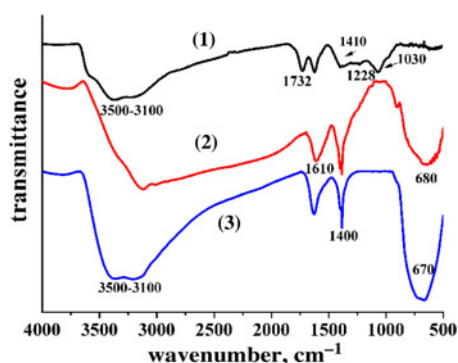


**Figure 2** FTIR spectra of (1) GO, (2) TiO<sub>2</sub>-RGO and (3) TiO<sub>2</sub> in the range of 4000–500 cm<sup>-1</sup>

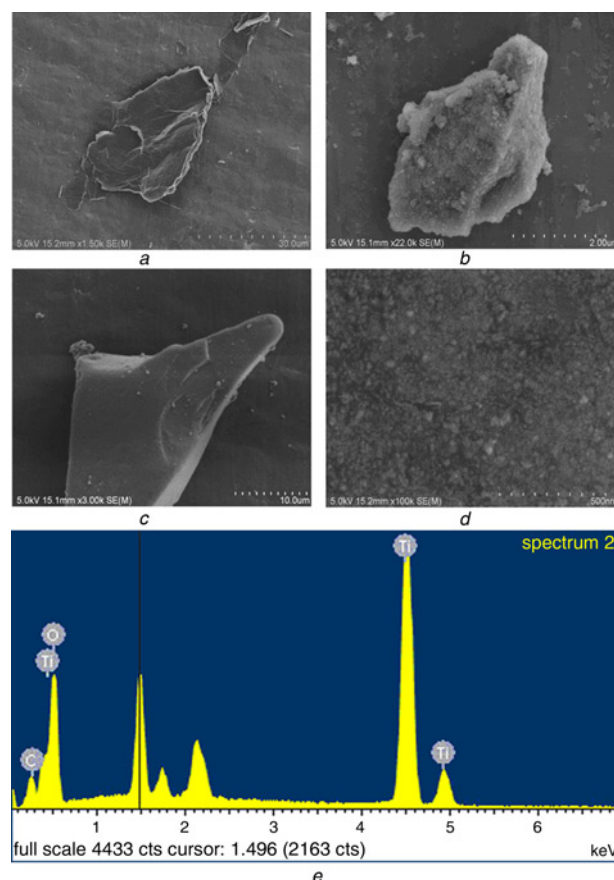


**Figure 3** SEM images of the as-prepared samples  
a GO, TiO<sub>2</sub>-RGO with different GO concentration  
b 0.2 g/l  
c and d 0.4 g/l  
e EDS confirms the presence of TiO<sub>2</sub> particles

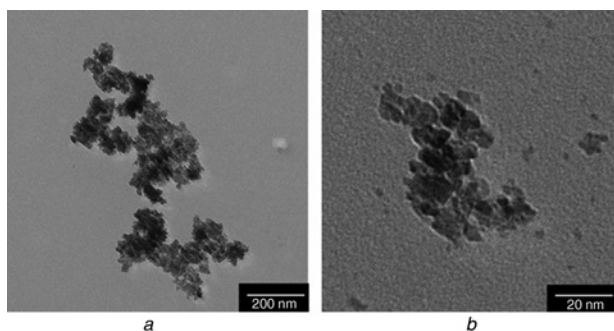


**Figure 4** TEM images of the  $\text{TiO}_2$  particles obtained by refluxing PTC solution at  $98^\circ\text{C}$  for 12 h

the GO surface became smooth and the wrinkles disappeared in the composites. This phenomenon indicated that some nanoparticles were well distributed on the RGO surface, which are also demonstrated by higher magnification SEM images (Fig. 3d). Elemental analyses confirmed that the nanoparticles were  $\text{TiO}_2$  in Fig. 3e. As shown in Figs. 3b and c, the  $\text{TiO}_2$  nanoparticles in the composites tended to aggregate into large particles with low GO concentration. Fig. 4 depicts the TEM micrographs of the  $\text{TiO}_2$  particles obtained by refluxing the PTC solution. The Figures clearly show that the  $\text{TiO}_2$  particles are round in shape, and the average diameter of the  $\text{TiO}_2$  particles is about 10 nm.

The photocatalytic activities of the as-prepared  $\text{TiO}_2$ -RGO and  $\text{TiO}_2$  were measured by the photodegradation of MB under UV light ( $\lambda = 254 \text{ nm}$ ), the results are shown in Fig. 5. The normalised temporal concentration changes ( $C/C_0$ ) of MB during photocatalytic degradation were proportional to the normalised maximum absorbance ( $A/A_0$ ). Therefore the degradation rate of MB could be obtained from the following equation

$$\eta = (A_0 - A)/A_0 \times 100\% \quad (1)$$

where  $A_0$  is the absorbance of the initial concentration of MB,  $A$  is the absorbance of concentration of MB after a given time reaction under UV light. It can be clearly seen from Fig. 5a that the  $\text{TiO}_2$ -RGO showed progress in the photocatalytic degradation of MB compared with neat  $\text{TiO}_2$ . Under UV light irradiation, 90% of the initial dye was decomposed for  $\text{TiO}_2$ -RGO after  $< 1.5 \text{ h}$  and nearly 45% of the initial dye still remained in the solution after the same time period for the as-prepared  $\text{TiO}_2$ . The  $\text{TiO}_2$ -RGO and  $\text{TiO}_2$  particles were filtered and dried at room temperature after photocatalytic degradation of MB under UV light, and then a fresh MB solution was added. As can be seen from Fig. 5b, there was no significant decrease in photocatalytic degradation and nearly 80% of the added dye was degraded by  $\text{TiO}_2$ -RGO after 2 h.

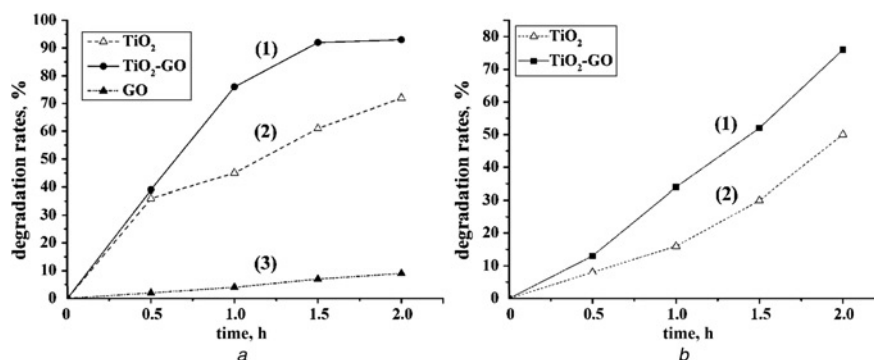


**Figure 5** Fig. 5a: photocatalytic degradation of MB under UV light over (1)  $\text{TiO}_2$ -RGO (GO concentration is 0.4 g/l), (2)  $\text{TiO}_2$  and (3) GO; Fig. 5b: over (1)  $\text{TiO}_2$ -RGO (GO concentration is 0.4 g/l) and (2)  $\text{TiO}_2$  during repeated uses (catalyst, 50 mg; initial concentration of MB, 5 mg/l; volume of MB, 150 ml)

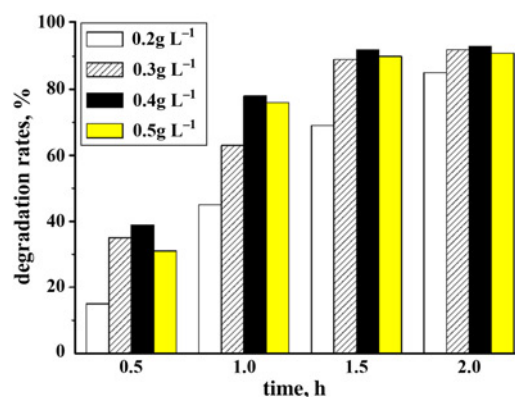


**Figure 6** Photocatalytic degradation of MB under UV light with different GO concentration (catalyst, 50 mg; initial concentration of MB, 5 mg/l; volume of MB, 150 ml)

The amount of RGO in the composite could be changed by adjusting the amount of the GO used in preparation of the composite. As shown in Fig. 6, the photocatalytic degradation activity of the  $\text{TiO}_2$ -RGO composites was enhanced with the increase of the reduced GO in the composite. The activity of the composites was the highest when the concentration of GO was 0.4 g/l. In addition, all the  $\text{TiO}_2$ -RGO composites showed much better photocatalytic degradation activity than pure  $\text{TiO}_2$ . As the content of the RGO in the composite increased, more  $\text{TiO}_2$  nanoparticles were loaded on the RGO surface. The rise of the RGO content in the composites could improve the adsorption capability of the composites, which led to the increase of reaction contact-area between photocatalyst and dye. Thus, the photocatalytic activity of the composites was enhanced. However, the black RGO in the composite could increase photo absorbing and scattering. As a result, the photocatalytic activity of the composites would decrease when the RGO content was too high [16].

The mechanisms of the  $\text{TiO}_2$ -RGO composites with high performance for photocatalytic degradation of MB under UV light are explained as follows. First, the RGO provide a good supporting substrate for the  $\text{TiO}_2$  nanoparticles and avoided the aggregation of  $\text{TiO}_2$  nanoparticles to a large degree in practical use. The second reason was that the RGO could increase the adsorption ability of the  $\text{TiO}_2$ -RGO catalyst. MB molecules could easily transfer from the solution to the catalysts surface, which promoted the process of photocatalytic degradation of dye. The third one was that the RGO played an important role in charge separation and transportation. Under UV light irradiation, the photoinduced electrons ( $e^-$ ) of  $\text{TiO}_2$  were transferred from the conduction band of  $\text{TiO}_2$  to RGO, and as a result, positive charged holes ( $h^+$ ) were formed. Thus, in the  $\text{TiO}_2$ -RGO composite, the RGO served as an acceptor of the

generated electrons of TiO<sub>2</sub> and suppressed the recombination of electrons (e<sup>-</sup>) with positive charged holes (h<sup>+</sup>), leaving more charge carriers to form reactive species and promote the degradation of dyes.

**4. Conclusions:** We successfully developed a novel method for the fabrication of TiO<sub>2</sub>-RGO composites with GO and PTC via thermal treatment. TiO<sub>2</sub> nanoparticles were uniformly distributed throughout the RGO surface through a chemical bond formed between the two components. The as-prepared TiO<sub>2</sub>-RGO composites exhibited high efficiency for degrading MB under UV light and the amount of RGO in the composite had significant influence on the photocatalytic degradation activity. The composite displayed the highest activity when the concentration of GO was 0.4 g/l. The enhanced effect of RGO on the photocatalytic properties was attributed to being a support for TiO<sub>2</sub>, the increase of adsorption ability and an electron acceptor suppressing charge recombination. The TiO<sub>2</sub>-RGO may find promising applications in addressing various environmental issues.

## 5 References

- [1] Hoffmann M.R., Martin S.T., Choi W.Y., Bahnemann D.W.: 'Environmental applications of semiconductor photocatalysis', *Chem. Rev.*, 1995, **95**, pp. 69–96
- [2] Sun C.Y., Zhao D., Chen C.C., Ma W.H., Zhao J.C.: 'TiO<sub>2</sub>-mediated photocatalytic debromination of decabromodiphenyl ether: kinetics and intermediates', *Environ. Sci. Technol.*, 2009, **43**, pp. 157–162
- [3] Shen X.T., Zhu L.H., Liu G.X., Yu H.W., Tang H.Q.: 'Enhanced photocatalytic degradation and selective removal of nitrophenols by using surface molecular imprinted titania', *Environ. Sci. Technol.*, 2008, **42**, pp. 1687–1692
- [4] An G.M., Ma W.H., Sun Z.Y., *ET AL.*: 'Preparation of titania/carbon nanotube composites using supercritical ethanol and their photocatalytic activity for phenol degradation under visible light irradiation', *Carbon.*, 2007, **45**, pp. 1795–1801
- [5] Woan K., Pyrgiotakis G., Sigmund W.: 'Photocatalytic carbon-nanotube-TiO<sub>2</sub> composites', *Adv. Mater.*, 2009, **21**, pp. 2233–2239
- [6] Velasco L.F., Parra J.B., Ania C.O.: 'Role of activated carbon features on the photocatalytic degradation of phenol', *Appl. Surf. Sci.*, 2010, **256**, pp. 5254–5258
- [7] Mu S., Long Y.Z., Kang S.Z., Mu J.: 'Surface modification of TiO<sub>2</sub> nanoparticles with a C<sub>60</sub> derivative and enhanced photocatalytic activity for the reduction of aqueous Cr(VI) ions', *Catal. Commun.*, 2010, **11**, pp. 741–744
- [8] Lu X., Imane T.: 'Demndrimer-mediated synthesis of water-dispersible carbon-nanotube-supported oxide nanoparticles', *J. Phys. Chem. C*, 2007, **111**, pp. 8459–8462
- [9] Rabin B., Peter K.Y., Stephen F.S.: 'Intercalation of polypyrrole into graphite oxide', *Synth. Met.*, 2006, **15**, pp. 1023–1027
- [10] Uhl F.M., Wilkie C.A.: 'Preparation of nanocomposites from styrene and modified graphite oxides', *Polym. Degradation Stab.*, 2004, **84**, pp. 215–226
- [11] Hammers W., Offeman R.: 'Preparation of graphitic oxide', *J. Am. Chem. Soc.*, 1958, **80**, p. 1339
- [12] Xu C., Wang X.: 'Fabrication of flexible metal-nanoparticle films using graphene oxide sheets as substrates', *Small.*, 2009, **5**, pp. 2212–2217
- [13] Ichinose M., Terasaki M., Katsuki H.: 'Properties of peroxotitanium acid solution and peroxo-modified anatase sol derived from peroxo-titanium hydrate', *J. Sol-Gel Sci. Technol.*, 2001, **22**, pp. 33–40
- [14] Zhang H., Lv X.J., Li Y.M., Wang Y., Li J.H.: 'P25-graphene composite as a high performance photocatalyst', *Nano.*, 2010, **4**, pp. 380–386
- [15] Khaled S.M., Sui R.H., Charpentier P.A., Rizkalla A.S.: 'Synthesis of TiO<sub>2</sub>-PMMA nanocomposite: using methacrylic acid as a coupling agent', *Langmuir.*, 2007, **23**, pp. 3988–3995
- [16] Jiang G.D., Lin Z.F., Chen C., *ET AL.*: 'TiO<sub>2</sub> nanoparticles assembled on graphene oxide nanosheets with high photocatalytic activity for removal of pollutants', *Carbon.*, 2011, **49**, pp. 2693–2701